# THE HYDRODYNAMIC EVOLUTION OF IMPULSIVELY HEATED CORONAL LOOPS: EXPLICIT ANALYTICAL APPROXIMATIONS

Markus J. Aschwanden<sup>1</sup> and David Tsiklauri<sup>2</sup>

### **ABSTRACT**

We derive simple analytical approximations (in explicit form) for the hydrodynamic evolution of the electron temperature T(s,t) and electron density n(s,t), for one-dimensional coronal loops that are subject to impulsive heating with subsequent cooling. Our analytical approximations are derived from first principles, using (1) the hydrodynamic energy balance equation, (2) the loop scaling laws of Rosner-Tucker-Vaiana and Serio, (3) the Neupert effect, and (4) the Jakimiec relationship. We compare our analytical approximations with 56 numerical cases of time-dependent hydrodynamic simulations from a parametric study of Tsiklauri et al., covering a large parameter space of heating rates, heating timescales, heating scale heights, loop lengths, for both footpoint and apex heating, mostly applicable to flare conditions. The average deviations from the average temperature and density values are typically  $\approx 20\%$  for our analytical expressions. The analytical approximations in explicit form provide an efficient tool to mimic time-dependent hydrodynamic simulations, to model observed soft X-rays and extreme-ultraviolet light curves of heated and cooling loops in the solar corona and in flares by forward fitting, to model microflares, to infer the coronal heating function from light curves of multi-wavelength observations, and to provide physical models of differential emission measure distributions for solar and stellar flares, coronae, and irradiance.

Key words: hydrodynamics – Sun: corona – Sun: UV radiation

## 1. INTRODUCTION

The physical understanding of observed electron densities and temperatures of solar coronal loops, in the quiet Sun and in active regions, in nanoflares and giant flares, is based on our concepts of heating and cooling processes. The inference of heating functions in the solar corona is still an elusive mystery, mostly because of the lack of suitable multi-wavelength observations with high spatial resolution, high cadence, and broad spectroscopic temperature coverage, while the cooling processes are better understood, in terms of thermal conduction and radiative loss processes. The problem can be modeled either with time-dependent hydrodynamic simulations or with analytical solutions. A large number of time-dependent onedimensional (1D) hydrodynamic simulations have been performed for coronal loops (e.g., Vesecky et al. 1979; Krall & Antiochos 1980; Peres et al. 1982; Craig et al. 1982; Mariska & Boris 1983; McClymont & Craig 1985a, 1985b; MacNeice 1986; Klimchuk et al. 1987; Klimchuk & Mariska 1988; Mok et al. 1991; Jakimiec et al. 1992; Robb & Cally 1992; Peres 1997; Betta et al. 1999; Reale et al. 2000a, 2000b; Warren et al. 2002; Winebarger et al. 2003a, 2003b; Spadaro et al. 2003; Tsiklauri et al. 2004; Winebarger & Warren 2004, 2005). A recent review is given in Section 4.7 of Aschwanden (2004). Hydrodynamic simulations calculate the evolution of temperature T(s, t) and density n(s, t) (or pressure p(s, t)) in time, by solving the hydrodynamic continuity, momentum, and energy equations. They have the disadvantage to be time-consuming, even for a single run and on fast computers, and thus forward fitting to observed light curves is an even more time-consuming process, because it would require many iterations. Thus, hydrodynamic simulations are, although accurate and powerful, an unpractical tool to infer information on the coronal heating function from observations.

On the other side, analytical work has been tackled to model the temperature and density of coronal loops, mostly focusing on stationary (hydrostatic) solutions, where the heating rate balances the energy losses by thermal conduction and radiation. The most seminal papers deal with hydrostatic solutions for (spatially) uniform heating (Rosner et al. 1978) and nonuniform base heating (Serio et al. 1981), resulting into scaling laws between the parameters of loop length, maximum temperature, and base density. Some generalizations include also the geometric divergence of loop diameters with height and nonuniform heating localized at the loop apex. A recent review of analytical solutions for hydrostatic loops is given in Section 3 of Aschwanden (2004). Analytical solutions of the time-dependent hydrodynamic equations have never been calculated in full generality, except for some special cases, such as steady-flow (or siphon-flow) solutions (e.g., Cargill & Priest 1980; Noci 1981), which is similar to the solar wind solution of Parker (1958). These special solutions, however, ignore the energy equation and temperature evolution. A recent review of work on timedependent solutions of the hydrodynamic equations is given in Section 4 of Aschwanden (2004).

It appears that a general solution of the time-dependent hydrodynamic equations is out of reach, even for a subset of a particular (time-dependent) heating function, and thus some suitable analytical approximations would be desirable for many purposes. Some analytical approximations, mostly of the cooling phase, have been formulated, e.g., by Fisher & Hawley (1990), Kopp & Poletto (1993), Cargill (1994), Cargill & Klimchuk (2004), but a complete approximation of the density and temperature evolution during the entire heating and cooling phase has been formulated only recently, in the so-called Enthalpy-Based Thermal Evolution of Loops (EBTEL) model by Klimchuk et al. (2008). The analytical approximation of the EBTEL code by Klimchuk et al. (2008) has the following advantages over the earlier work of Cargill (1994): (1) it allows for arbitrary heating time profiles, (2) treats radiative and conductive cooling simultaneously, and

<sup>&</sup>lt;sup>1</sup> Lockheed Martin Advanced Technology Center, Solar & Astrophysics Laboratory, Org. ADBS, Bldg. 252, 3251 Hanover Street, Palo Alto, CA 94304, USA; aschwanden@lmsal.com

<sup>&</sup>lt;sup>2</sup> Astronomy Unit, School of Mathematical Sciences, Queen Mary, University of London, Mile End Road, London, E1 4NS, UK; D.Tsiklauri@qmul.ac.uk Received 2009 June 10; accepted 2009 September 11; published 2009 October 29

(3) is tested by a numerical hydrodynamic code (with the 1D hydrodynamic code called Adaptively Refined Godunov Solver (ARGOS) developed at the Naval Research Laboratory (NRL)). However, the analytical approximation of the EBTEL code has three major restrictions: (1) it is a 0D loop treatment in terms of spatially averaged profiles of density n(t) and temperature T(t), (2) it is limited to spatially uniform heating, and (3) it is formulated in the form of differential equations (in terms of dp/dt, dT/dt, dn/dt) that need to be iterated in time, starting from a given initial condition.

In this study, we develop an analytical approximation to the hydrodynamic evolution of the temperature and density in impulsively heated 1D loops in explicit form, which does not require any time iteration or specification of an initial condition, but is directly expressed as an explicit function of the heating function parameters (heating rate  $H_0$ , heating timescale  $\tau_{\text{heat}}$ , and spatial heating scale height  $s_H$ ) and loop length (L). We derive physical key parameters directly from the hydrodynamic energy equation and approximate the time evolution with simple analytical functions. We compare the analytical approximations with numerical 1D hydrodynamic computations of a parametric study by Tsiklauri et al. (2004), carried out with the Lagrangian Re-map code by Arber et al. (2001). The derived analytical approximations in explicit form should be useful to mimic timedependent hydrodynamic simulations, to model observed light curves in soft X-rays and extreme-ultraviolet (EUV) of heated and cooling loops in the solar corona by forward fitting, as well as in flares, to infer the coronal heating function from light curves in multi-wavelength observations, and to provide physical models of differential emission measure (DEM) distributions for solar and stellar flares, coronae, and irradiance.

## 2. ANALYTICAL APPROXIMATIONS

## 2.1. The Energy Balance Equation

A basic hydrodynamic model of the evolution of a coronal loop consists of an initial heating phase with subsequent cooling by thermal conduction and radiation. The time-dependent hydrodynamic energy balance equation of a one-dimensional coronal loop as a function of time t and spatial coordinate s is generally expressed as

$$\rho T \frac{D}{Dt} S = E_H - E_R - \nabla F_C \,, \tag{1}$$

where S is the entropy per unit mass of the plasma,  $D/Dt = (\partial/\partial t + v \ \partial/\partial s)$  is the total derivative in space and time,  $\rho = nm \approx n_e m_p$  is the mass density,  $n_e$  is the electron number density, and  $m_p$  is the proton mass. The left-hand side describes the heat changes of the plasma due to heating and cooling processes, which are specified on the right-hand side: the volumetric heating rate  $E_H(s,t)$  (per volume and time unit), the radiative cooling rate  $E_R(s,t)$ , and the conductive cooling rate  $\nabla F_C$ , expressed as a function of the conductive flux  $F_C(s,t)$ . When a plasma is thermally isolated, so that there is no heat exchange with the ambient plasma, the thermodynamic state is called *adiabatic* and the *entropy* S is constant, so that the left side is zero,

$$0 = E_H - E_R - \nabla F_C. \tag{2}$$

Our approach is to subdivide the time evolution into two time phases of either dominant heating or cooling (Figure 1). For an impulsive heating process, the heating rate is initially approximately balanced by thermal conduction, where radiative

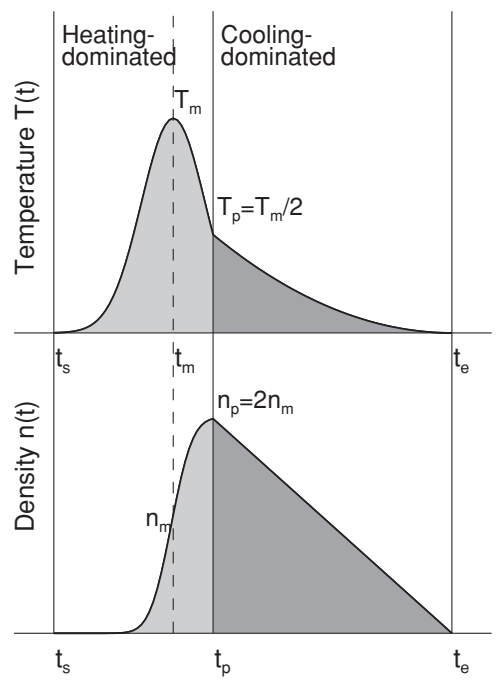


**Figure 1.** Generic time evolution of temperature T(t) and electron density n(t) during an impulsive heating process with subsequent cooling, subdivided into two time phases of (1) dominant heating  $(t_s < t < t_p)$  and (2) dominant cooling  $(t_p < t < t_e)$ . The maximum of the temperature profile  $T_m = T(t = t_m)$  occurs at time  $t_m$ , and the density has a peak value  $n_p = n_e(t = t_p)$  at time  $t_p$ , approximately when the temperature drops to half of the maximum value, i.e.,  $T_p = T_m/2$ .

loss can be neglected, followed by subsequent cooling, where initially the conductive loss rate is dominant (if the plasma is sufficiently hot), while the radiative cooling rate dominates later on. Thus, we can neglect the radiative cooling during the heating phase, and the heating term during the cooling phase,

$$E_H - \nabla F_C \approx 0$$
 for  $t_s \leqslant t \leqslant t_p$ , (3)

$$-E_R - \nabla F_C \approx 0$$
 for  $t_p \leqslant t \leqslant t_e$ , (4)

where we denote  $t_s$  as the start time of heating,  $t_p$  the density peak time, and  $t_e$  the end time. Neglecting some of the non-dominant terms in each respective time phase renders the energy balance equation more treatable for an analytical solution in explicit form.

In the following, we quantify the three terms of the energy equation. The first term is the heating rate  $E_H(s,t)$ , which is an unknown function in the solar corona, but is often thought to be impulsive that can be approximated with a single-peaked function in time, such as with a Gaussian, for an elementary heating process. Also the spatial heating dependence is completely unknown, but the most frequent parameterizations include a spatially constant (uniform) heating function, or heating functions concentrated either at the loop footpoint or at the loop apex, falling off exponentially with distance. Thus, we can parameterize the heating rate for these three cases as

$$E_{H}(s,t) = H_{0} \exp\left(-\frac{(t-t_{m})^{2}}{2\tau_{\text{heat}}^{2}}\right) \exp\left(-\frac{s}{s_{H}}\right)$$

$$\times \begin{cases} s_{H} > 0 & \text{for footpoint heating} \\ s_{H} = \infty & \text{for uniform heating} \\ s_{H} < 0 & \text{for apex heating,} \end{cases}$$
 (5)

where  $t_m$  is the time of maximum heating,  $\tau_{\text{heat}}$  is the Gaussian width of the heating time interval,  $s_H$  is the heating scale height, and  $H_0$  is the volumetric heating rate at the footpoint.

Equation (5) is a unified definition for all three cases, where the heating scale height  $s_H$  is positive for footpoint heating, negative for apex heating, and infinite for uniform heating.

The next term in the energy equation is the conductive loss rate  $\nabla F_C$ , which is expressed as the divergence of the conductive flux  $F_C$ .

$$F_C(s) = \left[ -\kappa T^{5/2}(s) \frac{dT(s)}{ds} \right] = -\frac{2}{7} \kappa \frac{d}{ds} [T^{7/2}(s)], \quad (6)$$

where the temperature profile T(s) refers to a particular time t (but T(s,t) is time-dependent in general), and  $\kappa = 9.2 \times 10^{-7}$  (erg s<sup>-1</sup> cm<sup>-1</sup> K<sup>-7/2</sup>) is the *Spitzer* conductivity. Thus, the conductive flux depends only on the temperature and spatial loop size, but not on the electron density n(s,t).

The other loss term in the energy balance equation is the radiative loss rate  $E_R$ , which can be written as a product of densities and a temperature-dependent function, called the radiative loss function  $\Lambda(T)$ , for optically thin plasmas,

$$E_R = n_e n_p \Lambda(T) \approx n^2 \Lambda(T), \tag{7}$$

where the coronal approximation of fully ionized plasma is used ( $n \approx n_p \approx n_e$ ). The radiative loss function  $\Lambda(T)$  is usually approximated by piecewise power laws. Here we are only interested in the coronal temperature range  $T \gtrsim 1.0$  MK, for which the following approximations are commonly used (e.g., Rosner et al. 1978):

$$\Lambda(T) \approx \begin{cases} 10^{-21.94} & \text{for } 10^{5.8} < T < 10^{6.3} \text{ (EUV)} \\ 10^{-17.73} T^{-2/3} & \text{for } 10^{6.3} < T < 10^{7.6} \text{ (SXR)}. \end{cases}$$

Thus, the entire coronal temperature range seen in soft X-rays (i.e.,  $2.0 \lesssim T \lesssim 40$  MK) can be approximated with a single power law  $\Lambda(T) \propto T^{-2/3}$ , while the radiative loss rate in the EUV range (i.e.,  $0.6 \lesssim T \lesssim 2.0$  MK) is essentially constant. Now, with Equations (2)–(8) we have defined the basic relations to analytically derive the temperature and density evolution of a heated and cooling coronal loop.

## 2.2. Temperature Profile During the Heating Phase

To derive the temperature profile during the heating phase (for a given time t), we essentially balance the heating rate  $E_H(s)$  (Equation (5)) with the conductive loss rate  $\nabla F_C(s)$  (Equation (6)), as expressed in Equation (3), which yields a differential equation of second order in the spatial coordinate s,

$$E_H(s) = \frac{d}{ds} \left[ -\kappa T^{5/2}(s) \frac{dT(s)}{ds} \right] = -\frac{2}{7} \kappa \frac{d^2 T(s)^{7/2}}{ds^2}.$$
 (9)

This second-order differential equation can be turned into a double-integral equation by expressing it as an explicit function of T(s),

$$T(s) = \left[ \int ds \, \int -\frac{7}{2\kappa} E_H(s) \, ds \right]^{2/7}.$$
 (10)

For the case of uniform heating, the heating rate  $E_H(s, t = t_m) = H_0$  is a constant along the space coordinate s, and the integration yields two integration constants  $c_1$  and  $c_2$ ,

$$T^{\text{uni}}(s) = \left[ -\frac{7H_0}{4\kappa} s^2 + c_1 s + c_2 \right]^{2/7}, \tag{11}$$

which can be determined from the boundary conditions at the loop footpoint,  $T(s = 0) = T_1$ , and at the loop apex,  $T(s = L) = T_2$ , yielding the temperature profile

$$T^{\text{uni}}(s) = \left[ -\frac{7H_0}{4\kappa} s^2 + \left( \frac{T_2^{7/2} - T_1^{7/2}}{L} + \frac{7H_0}{4\kappa} L \right) s + T_1^{7/2} \right]^{2/7}.$$
(12)

Since the temperature boundary at the loop footpoint is in the cool chromosphere, with a typical temperature of  $T_1 \approx 2 \times 10^4$  K in the temperature minimum region, which is much lower than the coronal temperatures of  $T_2 \gtrsim 10^6$  K at the loop apex, we have  $T_1 \ll T_2$  and can readily neglect the terms with  $T_1$ ,

$$T^{\rm uni}(s) \approx T_2 \left[ \frac{s}{L} + \frac{7H_0L^2}{4\kappa T_2^{7/2}} \left( \frac{s}{L} \right) \left( 1 - \frac{s}{L} \right) \right]^{2/7}.$$
 (13)

Assuming, furthermore, that the thermal conduction vanishes at the loop top for symmetric loops, we have a further boundary condition,

$$\frac{dT(s=L)}{ds} = 0, (14)$$

which constrains the heating rate  $H_0$  as a function of the loop apex temperature  $T_2$  and loop length L, i.e., by applying Equation (14) to Equation (13),

$$H_0^{\text{uni}} = \frac{4}{7} \kappa \frac{T_2^{7/2}}{L^2},\tag{15}$$

which is essentially the second scaling law derived in Rosner et al. (1978), except for the numerical factor  $(4/7)\kappa \approx 0.53 \times 10^{-6}$  that is about a factor of 2 lower due to the neglect of the radiate loss rate during the heating phase. Inserting this heating rate (required for symmetric loops) into the temperature profile (Equation (13)), we can express the temperature profile of uniformly heated loops simply as

$$T^{\text{uni}}(s) = T_2 \left[ \left( \frac{s}{L} \right) \left( 2 - \frac{s}{L} \right) \right]^{2/7}, \tag{16}$$

which is shown in Figure 2, where the symmetry of the loop is most evident, since T(s) = T(2L - s). A comparison with the Rosner–Tucker–Vaiana (RTV) solution (Rosner et al. 1978; Equation (C1) therein) shows that our simpler approximation (neglecting radiative loss during the heating phase) is fully adequate for all practical applications (see Figure 2).

Vice versa, Relation (15) can be used to predict the maximum loop temperature  $T_2$  based on the maximum heating rate  $H_0$  and loop length L,

$$T_2^{\text{uni}} = \left\lceil \frac{7L^2 H_0}{4\kappa} \right\rceil^{2/7},\tag{17}$$

for the case of uniform heating.

Now we are generalizing the same calculation of the temperature profile T(s) for non-uniform heating, by including the heating scale height  $s_H$  defined in Equation (5), which yields for the temperature profile (in analogy to  $T^{\rm uni}(s)$  in Equation (11)),

$$T(s) = \left[ -\frac{7}{2\kappa} H_0 \, s_H^2 \exp\left(-\frac{s}{s_H}\right) + c_1 s + c_2 \right]^{2/7}. \tag{18}$$

Substituting the integration constants  $c_1$  and  $c_2$  from the boundary conditions  $T(s=0)=T_1\ll T_2$  and  $T(s=L)=T_2$  yields

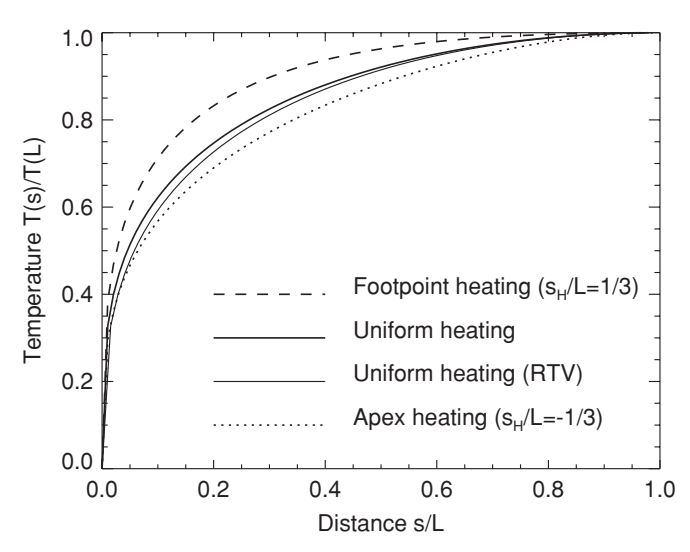


**Figure 2.** Analytical solutions of the temperature profile T(s) is shown for uniform and non-uniform heating (for a heating scale height ratio of  $s_H/L=1/3$  at the footpoint, and  $s_H/L=-1/3$  at the apex). For comparison, we show also the analytical solution for uniform heating calculated by Rosner et al. (1978), which includes also radiative loss.

then (in analogy to Equation (13))

$$T(s) = T_2 \left[ \left( \frac{s}{L} \right) + \frac{7H_0 s_H^2}{2\kappa T_2^{7/2}} \left( 1 - \exp\left( -\frac{s}{s_H} \right) - \left( \frac{s}{L} \right) \right) \right] \times \left[ 1 - \exp\left( -\frac{L}{s_H} \right) \right] \right]^{2/7}.$$
 (19)

Requiring symmetric loops with vanishing thermal conduction at the apex (Equation (14)), we then obtain a condition for the heating rate (in analogy to Equation (15)),

$$H_0 = H_0^{\text{uni}} q_H = \frac{4\kappa T_2^{7/2} q_H}{7L^2},\tag{20}$$

where we define a heating non-uniformity factor  $q_H$ , which only depends on the ratio  $s_H/L$  and is unity for uniform heating,

$$q_H = \frac{L^2}{2s_H^2} \frac{1}{[1 - (1 + L/s_H)\exp(-L/s_H)]},$$
 (21)

which yields the loop profile expressed as a function of  $T_2$ ,  $s_H$ , and L.

$$T(s) = T_2 \left[ \left( \frac{s}{L} \right) + 2q_H \left( \frac{s_H}{L} \right)^2 \left( 1 - \exp\left( -\frac{s}{s_H} \right) - \left( \frac{s}{L} \right) \right) \right] \times \left[ 1 - \exp\left( -\frac{L}{s_H} \right) \right] \right]^{2/7}.$$
 (22)

Expanding the exponential function in Equation (22) to second order, i.e.,  $\exp(-x) = 1 - x + x^2/2! - \cdots$ , one can show that the asymptotic case of  $s_H \mapsto \infty$  lets the *heating non-uniformity factor*  $q_H$  converge to unity, the non-uniform temperature profile T(s) (Equation (22)) converges to the uniform temperature profile  $T^{\text{uni}}(s)$  (Equation (16)), and the heating rate  $H_0$  (Equation (20)) converges to  $H_0^{\text{uni}}$  (Equation (15)) for uniform heating. An example of the analytical temperature profile T(s) (Equation (22)) is shown in Figure 2 for footpoint heating with a heating scale height ratio of  $s_H/L = 1/3$ , which is about

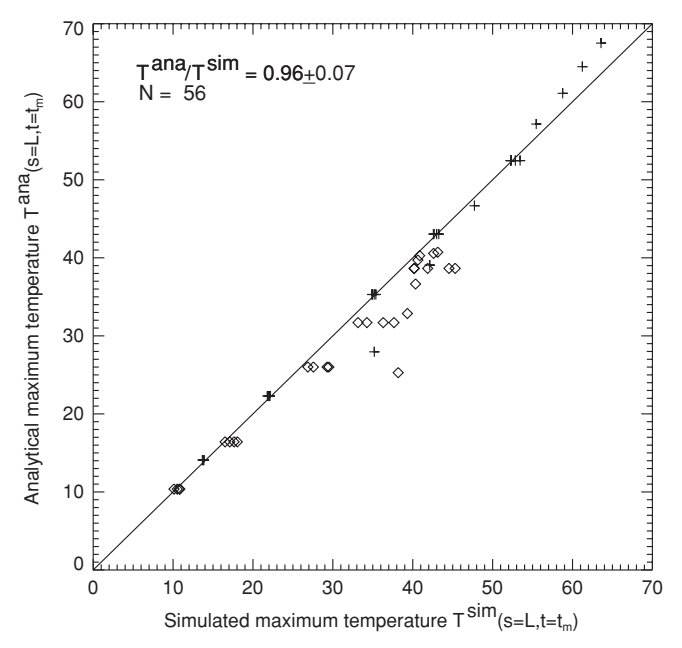


**Figure 3.** Comparison of analytical solutions of the maximum temperature  $T_m = T(s = L, t = t_m)$  at the loop apex with the values obtained from numerical hydrodynamic simulations. The temperature values agree within a few percents for both apex (crosses) and footpoint heating (diamonds).

the shortest stable heating scale height (Serio et al. 1981). The temperature profile is clearly flatter than for uniform heating. Alternatively, we show also an example for apex heating, with  $s_H/L = -1/3$ , which exhibits a steeper temperature gradient throughout the loop. This solution for a temperature profile with non-uniform heating and exponential heating scale height has also been calculated in Priest et al. (2000, Appendix A, Equation (A3)), which agrees with our solution (Equation (22)).

Vice versa, we can use the condition of Equation (20) to express the loop top temperature  $T_2$  as a function of the heating rate for the general case of non-uniform heating,

$$T_2 = T_2^{\text{uni}} q_H^{2/7} = \left[ \frac{7L^2 H_0}{4\kappa q_H} \right]^{2/7}$$
 (23)

In Figure 3, we show a comparison of the analytical approximations of the maximum temperatures  $T^{\text{ana}}$  (s = L, t = $t_m$ ) =  $T_2$  (Equation (23)) with numerically calculated values  $T^{\sin s}(s = L, t = t_m)$  from hydrodynamic simulations of Tsiklauri et al. (2004). We find a satisfactory agreement of  $T^{\rm ana}/T^{\rm sim}=0.96\pm0.07$  within about 10% for this set of 56 simulations, covering four different heating timescales  $\tau_{\text{heat}}$ , five heating rates  $E_H$ , eight loop lengths L, two heating scale heights  $s_H$ , with footpoint as well as loop top heating. (However, because the numerical simulations of Tsiklauri et al. (2004) slightly deviate in the definition of the spatial heating function, simulating a Gaussian rather than an exponential one (Equation (5)) used here, we find a small difference in the maximum temperature  $T_2$  for the case of apex heating, which we correct with an empirical factor of (4/3), so  $T_2^{\text{Tsiklauri, apex}} =$  $(4/3)T_2$ .)

## 2.3. Temperature Evolution During the Heating Phase

The temperature profiles T(s) calculated above show that the loop top temperature  $T_2$  is only a function of the heating rate  $H_0$  and loop length L, in the case of uniform heating

(Equation (17)), and in addition of the heating scale height  $s_H$ , in the case of non-uniform heating (Equations (21) and (23)). This behavior is a result of the energy balance between heating and thermal conduction. If we assume approximate energy balance during each time step of the heating phase (which may not apply for very short heating timescales, when the heating timescale is significantly shorter than the conductive cooling time), we can then relate the time evolution of the loop top temperature  $T_2(t)$  (Equation (23)) to the time evolution of the heating function  $E_H(t)$  (Equation (5)),

$$T(s = L, t) = T_m \left[ \exp\left(-\frac{(t - t_m)^2}{2\tau_{\text{heat}}^2}\right) \right]^{2/7},$$
 (24)

where the maximum temperature  $T_m$  (at the loop apex s = L and maximum heating time  $t_m$ ), called  $T_2$  in Equation (23), is defined by

$$T_m = T(s = L, t = t_m) = \left[\frac{7L^2H_0}{4\kappa q_H}\right]^{2/7},$$
 (25)

with the constant  $q_H(s_H, L)$  being unity for uniform heating, but larger (smaller) than unity for footpoint (apex) heating according to the definition given in Equation (21). This is our approximation of the temperature function in explicit form for the time interval  $t_s < t < t_p$  of the heating phase.

In order to define a start time  $t_s$  of the heating process, we require that a significant heating rate has to be reached at the start to produce a loop temperature that exceeds the ambient coronal temperature  $T_0$ , say  $T_0 \approx 1.0$  MK. Using this requirement, Equation (24) yields the following start time  $t_s$ ,

$$t_s = t_m - \tau_{\text{heat}} \sqrt{7 \ln \left( T_m / T_0 \right)}, \tag{26}$$

which amounts to a rise time of about 4–5 heating timescales for a maximum temperature of  $T_m \approx 10$ –30 MK.

### 2.4. Particle Density Evolution During the Heating Phase

The evolution of the electron density n(t) in the loop can be understood in terms of the *Neupert effect*, which in essence states that the accumulated density in a heated loop is an integral function of the heating rate (e.g., Brown 1973; Veronig et al. 2005), because the chromospheric evaporation rate into the coronal loop is a function of the chromospheric heating rate or energy input,

$$n(t) \propto \int_0^t E_H(t') \left(\frac{dn_{\text{evap}}}{dE_H}\right) dt',$$
 (27)

where  $(dn_{\text{evap}}/dE_H)$  is the evaporation rate per heating power. If we neglect cooling during the heating phase, free energy is continuously added to the loop in the form of evaporating material, which increases the density in the loop monotonously, peaking at the end of the heating phase (at time  $t=t_p$ ). Numerical hydrodynamic simulations of the chromospheric evaporation process have been conducted for two different drivers (or heating scenarios): for non-thermal particle precipitation (e.g., Somov et al. 1981; Bloomberg et al. 1977; MacNeice et al. 1984; Nagai & Emslie 1984; Fisher et al. 1985a, 1985b, 1985c; Mariska & Poland 1985) and for heat conduction from the loop top (e.g., Nagai 1980; Somov et al. 1982; Cheng et al. 1984; Pallavicini & Peres 1983; MacNeice 1986; Fisher 1989; Mariska et al. 1989;

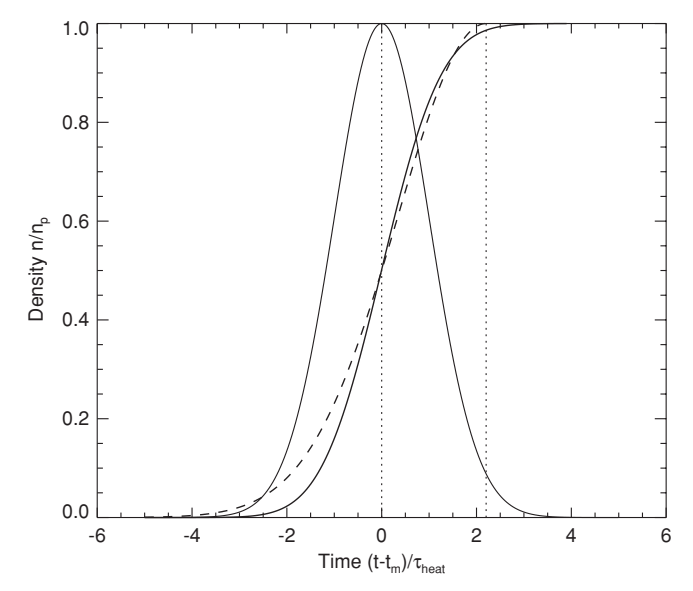


**Figure 4.** Heating rate  $E_H(t)$  is given by a Gaussian function (thin solid curve). The density function n(t) follows the time integral (thick solid curve) of this Gaussian function (for a constant value of  $dn_{\rm evap}/dE_H$ ) according to the Neupert effect, which can be approximated by a semi-Gaussian function (dashed curve). The time  $t_m$  of the maximum heating rate and the time  $t_p$  of the peak density are indicated with dotted lines.

Gan et al. 1991; Falchi & Mauas 2002), which all show a monotonic average density increase in the coronal loops until the end of the heating phase.

For a temporally symmetric heating function  $E_H(t)$ , like the (temporal) Gaussian heating function used in the numerical simulation (shown in Figure 1, top), the density increases in the time integrals (Equation (27)) before and after the heating maximum time  $t_m$ , by identical amounts due to the time symmetry of  $E_H(t)$ ,

$$n_{m} = n(t \leqslant t_{m}) = \int_{0}^{t_{m}} E_{H}(t') \left(\frac{dn_{\text{evap}}}{dE_{H}}\right) dt'$$
$$= n(t \geqslant t_{m}) = \int_{t_{m}}^{\infty} E_{H}(t') \left(\frac{dn_{\text{evap}}}{dE_{H}}\right) dt', \qquad (28)$$

and thus the value of the density  $n_m = n(t = t_m)$  at the heating maximum time  $t_m$  is expected to be half of the value  $n_p = n(t = t_p)$  of the final peak density  $n_{\max}$ , which is reached approximately at density peak time  $t_p$  (see Figure 4). So we have the relationship

$$n_m = n(t = t_m) = \frac{1}{2}n(t = t_p) = \frac{n_p}{2}$$
 (29)

due to the temporal symmetry of the heating function in the integral (Equation (27)). The average pressure in the loop increases during the heating phase and reaches a maximum and the density peak time  $t_p$  (as we verified in numerical hydrodynamic simulations), so that we can approximate it with a constant during this time interval  $(t_m \le t \le t_p)$ ,

$$p_m = p(t = t_m) = 2n_m k_B T_m \approx p(t = t_p) = 2n_p k_B T_p$$
. (30)

The latter two relations (Equations (29) and (30)) imply that the temperature dropped by about a factor of 2 at the density peak time (as illustrated in Figure 1),

$$T_p = T(t = t_p) \approx T_m \frac{n_m}{n_p} = \frac{T_m}{2}.$$
 (31)

In other words, since the average density and temperature vary reciprocally in an adiabatic loop, the temperature drops to half the maximum value while the density doubles at the peak time. Since we have already an analytical approximation T(t) for the temperature evolution in Equation (24), we can derive an analytical expression for the time interval  $t_p - t_m$  when the temperature drops to half of its maximum value  $T_m = T(t = t_m)$ . Setting the temperature to the half-maximum value in Equation (24), i.e.,  $T(t_p) = T(t_m)/2$ , we obtain the density peak time  $t_p$ ,

$$t_p = t_m + \tau_{\text{heat}} \sqrt{7 \ln 2} \approx t_m + 2.2 \tau_{\text{heat}},$$
 (32)

so it is about two Gaussian heating timescales after the temperature maximum time  $t_m$ . The time interval  $2(t_p - t_m)$  corresponds to the FWHM of the temperature profile T(s), since  $T(t = t_p) = T(t = t_m)/2$ .

For an analytical approximation of the density evolution n(t), we could make an ansatz with an integral function of the heating function as expressed in Equation (27), which requires also the knowledge of the evaporation rate per heating power,  $(dn_{\rm evap}/dE_H)$ . Assuming a constant value for  $(dn_{\rm evap}/dE_H)$ , the integral (Equation (27)) yields a monotonically increasing function, which can be well approximated by the left-hand side of a semi-Gaussian function,

$$n(t) \approx n_p \exp\left(-\frac{(t-t_p)^2}{2\tau_{\text{evap}}^2}\right)$$
 for  $t \leqslant t_p$ , (33)

with a Gaussian half-width that we call the evaporation timescale  $\tau_{\text{evap}}$ , which is defined by the requirement of Equation (29), i.e.,  $n_m = n_p/2$  in Equation (33),

$$\tau_{\text{evap}} = \frac{(t_p - t_m)}{\sqrt{2 \ln 2}} = \sqrt{7/2} \, \tau_{\text{heat}} \approx 1.87 \, \tau_{\text{heat}}.$$
 (34)

A comparison of the time integral of a Gaussian heating rate with the semi-Gaussian approximation is shown in Figure 4, which shows that the difference is always less than 10% of the peak density. The semi-Gaussian approximation has the same basic properties as the time integral of the Gaussian heating function: it is (1) monotonously increasing, (2) has the steepest slope at time  $t_m$ , and (3) asymptotically approaches the maximum value at  $t = t_p$ . Thus, the density profile n(t) (Equation (33)) increases monotonously up to the maximum value  $n_p$  during the dominant heating phase ( $t < t_p$ ), as shown in Figure 1 (bottom left).

Comparing this analytical approximation also with exact solutions of the density evolution n(t) computed by numerical hydrostatic codes (Tsiklauri et al. 2004), we find that a semi-Gaussian function is an adequate approximation during the dominant heating phase ( $t \le t_p$ ) for most practical purposes (as shown in the following), which justifies also our approximation of a constant evaporation rate ( $dn_{\text{evap}}/dE_H$ ) in the time integral of Equation (27).

## 2.5. The Peak Density

The density evolution n(t) in Equation (33) is expressed with three variables, the peak density value  $n_p$ , the peak time  $t_p$  (Equation (32)), and the evaporation timescale  $\tau_{\rm evap}$  (Equation (34)), which is a direct function of the heating timescale  $\tau_{\rm heat}$ . In order to obtain an analytical expression for the density peak value  $n_p$ , we are using the RTV (Rosner et al. 1978) and Serio's loop scaling law for hydrostatic loops with

non-uniform heating in a stratified atmosphere (Serio et al. 1981). Since these scaling laws are derived for the condition of energy balance between heating and conductive and radiative losses (Equation (2)), they generally apply to stationary loops in hydrostatic equilibrium. They are also approximately valid for impulsively heated loops with sufficiently long heating timescales, especially when the heating timescale is significantly longer than the conductive (and radiative) cooling timescales, because an energy balance is almost reached at the density peak time. Thus, we employ Serio's scaling law to find the maximum density, at least for long heating timescales. For short heating timescales, however, the maximum density predicted by the RTV or Serio's scaling law is not fully obtained, which we correct with a dynamical correction factor that scales with the ratio of the heating time to the loop filling time (see Equation (42)).

For the case of uniform heating and constant pressure, the relationship between loop pressure p, loop apex temperature  $T_2$ , and loop half-length L is given by the well-known RTV scaling law (Rosner et al. 1978),

$$p_1^{\text{RTV}} = p_2^{\text{RTV}} = \frac{1}{L} \left( \frac{T_2}{1400} \right)^3.$$
 (35)

(Here we label the footpoint position with the index 1 and the apex position with the index 2.) For the case of non-uniform heating (with a spatial heating scale height  $s_H$ , exponentially falling off above the footpoints) and gravitational stratification, the loop scaling law was generalized by Serio et al. (1981) to

$$p_1^{\text{Serio}} = p_1^{\text{RTV}} \exp\left(0.24 \frac{L}{s_H} + 0.12 \frac{L}{\lambda_T}\right),$$
 (36)

where  $\lambda_T$  is the pressure scale height

$$\lambda_T = \frac{2k_B T_2}{\mu m_H g_{\odot}} \approx 4.7 \times 10^9 \left(\frac{T_2}{1 \text{ MK}}\right) \text{ cm}, \quad (37)$$

with  $k_B$  the Boltzmann constant,  $\mu$  the mean molecular weight ( $\mu \approx 1.27$  for a hydrogen-to-helium abundance of 10),  $m_H$  the mass of the hydrogen atom, and  $g_{\odot}$  the solar gravitation. The apex pressure  $p_2$  is according to Serio's definition,

$$p_2^{\text{Serio}} = p(s = L) \approx p_1^{\text{Serio}} \exp\left(-\frac{H}{\lambda_T}\right),$$
 (38)

where  $H = [L/(\pi/2)] \cos \vartheta$  is the height of the loop, with  $\vartheta$  the inclination angle of the loop plane with respect to the vertical to the solar surface. The electron density  $n_2 = n(s = L)$  at the loop apex derives from the apex pressure according to the ideal gas law,

$$n_2^{\text{Serio}} = n(s = L) = \frac{p_2^{\text{Serio}}}{2k_B T_2}.$$
 (39)

The peak density derived from the RTV or Serio's scaling law applies strictly only for hydrostatic equilibrium, which is a stationary state that is obtained in the limit of constant heating (i.e., a heating time of  $\tau_{\text{heat}} \mapsto \infty$ ). Here, however, we deal with impulsive heating that may have heating timescales  $\tau_{\text{heat}}$  that are shorter than the evaporation timescale or cooling timescale. A crucial criterion whether the steady-state density is reached at the loop apex is the loop filling time by chromospheric evaporation, which is approximately the loop half-length L divided by the sound speed  $c_s$ ,

$$\tau_{\text{fill}} = \frac{L}{c_c},\tag{40}$$

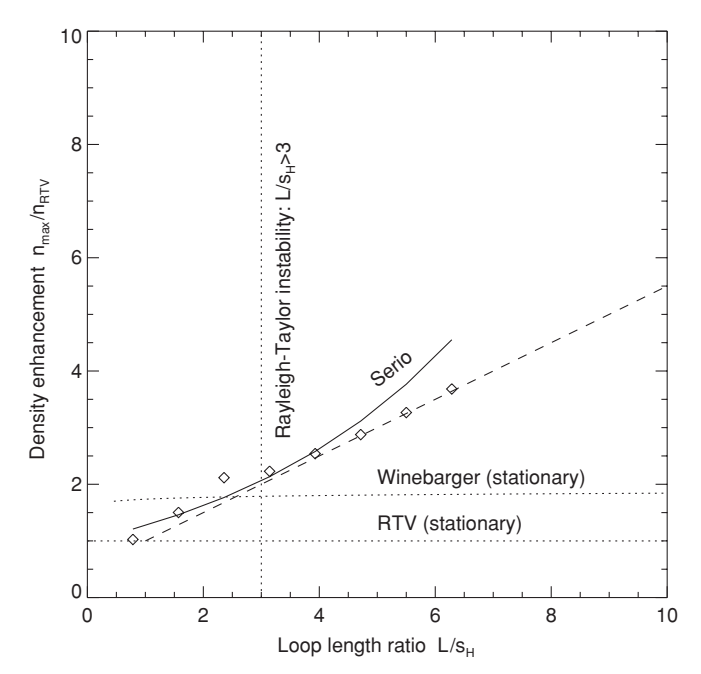


**Figure 5.** Maximum density enhancement with respect to the RTV density,  $n_P/n_{\rm RTV}$  as a function of the ratio of loop half-length to heating scale height,  $L/s_H$ , for a set of eight hydrodynamic numerical simulations performed by Tsiklauri et al. (2004), for  $s_H = 8.75$  Mm and loop half-lengths of  $L = 9, \ldots, 55$  Mm (diamonds). The scaling law of Serio et al. (1981) yields consistent predictions for  $L/s_H \gtrsim 3$ , but overpredicts the density enhancements for higher values of  $L/s_H \gtrsim 3$  where no stationary loop solutions exist due to the Rayleigh–Taylor instability. Numerical hydrodynamic simulations yield maximum density enhancements of  $n_P/n_{\rm RTV} \lesssim 2$  for stationary solutions (Winebarger et al. 2003a, 2003b). For dynamic simulations of impulsive heating and subsequent cooling maximum (Tsiklauri et al. 2004), maximum density enhancements of  $n_{\rm max}/n_{\rm RTV} \approx 0.5(1 + L/s_H)$  are obtained.

$$c_s = 1.66 \times 10^4 \sqrt{T_e/\mu}$$
 cm s<sup>-1</sup>. (41)

If the heating time  $\tau_{heat}$  is shorter than the sound crossing time  $\tau_{fill}$ , we expect that only a fraction  $\tau_{heat}/\tau_{fill}$  of the loop is filled with evaporated plasma, while for very long heating times we expect the steady-state solution with the maximum densities calculated by RTV (for uniform heating) or by Serio et al. (1981) for non-uniform heating. A simple approximation is an exponential function that asymptotically approaches the steady-state limit,

$$q_n^{\text{dyn}} = 1 - \exp\left[-\tau_{\text{heat}}/\tau_{\text{fill}}\right]. \tag{42}$$

Thus, applying this dynamic correction factor, we expect approximate peak densities  $n_p$  at the density peak time  $t=t_p$  of

$$n_p = n(t = t_p) = n_2^{\text{Serio}} q_n^{\text{dyn}}.$$
 (43)

The loop scaling law of Serio et al. (1981) is restricted to heating scale heights of  $s_H \gtrsim L/3$ , because a density inversion occurs for shorter scale heights that is unstable to the Rayleigh–Taylor instability. Therefore, there are no stationary solutions for  $L/s_H \gtrsim 3$ , as verified by hydrodynamic numerical simulations, which yield density enhancements of only  $n_{\rm max}/n_{\rm RTV} \lesssim 2$  (Winebarger et al. 2003a). Here we compare with the maximum densities obtained in the hydrodynamic simulations of Tsiklauri et al. (2004) and find the following empirical limit (Figure 5) for footpoint heating

$$n_{\rm max}^{foot} \approx n_{\rm RTV} \times 0.5 \left(1 + \frac{L}{s_H}\right),$$
 (44)

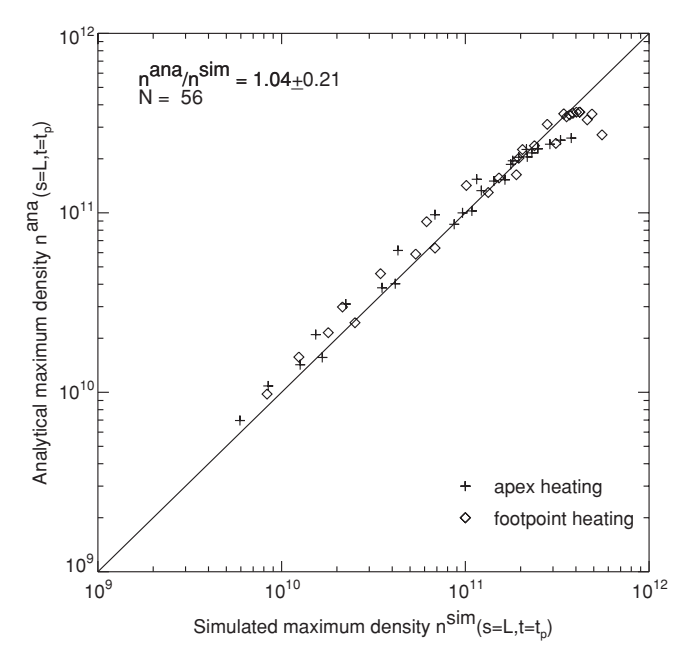


**Figure 6.** Comparison of analytical solutions of the peak density  $n_p = n(s = L, t = t_p)$  at the loop apex (Equations (45)) with the values obtained from numerical hydrodynamic simulations. The peak density values agree within a few percents for both apex (crosses) and footpoint heating (diamonds).

and the following constant for apex heating

$$n_{\rm max}^{apex} \approx n_{\rm RTV} \times 0.7.$$
 (45)

In summary, we find the following analytical approximations for the peak density  $n_p = n(s = L, t = t_p)$  at the loop apex for the different cases:

$$n_{p} = n_{\text{RTV}} \ q_{n}^{\text{dyn}}$$

$$\times \begin{cases} \exp(0.24L/s_{H} + 0.12L/\lambda_{T}) \\ \text{for } s_{H} > 0 \text{ (footpoint heating) and } L/s_{H} < 3 \\ \exp[0.5(1 + L/s_{H})] \\ \text{for } s_{H} > 0 \text{ (footpoint heating) and } L/s_{H} \geqslant 3 \\ 0.7 \quad \text{for } s_{H} < 0 \text{ (apex heating)} \\ 1.0 \quad \text{for uniform heating.} \end{cases}$$

$$(46)$$

In Figure 6, we show these theoretically predicted values  $n_p^{\rm ana}(s=L,t=t_p)$  as a function of the exact values  $n_p^{\rm sim}(s=L,t=t_p)$  obtained from numerical hydrodynamic simulations of a parametric study with 56 cases (Tsiklauri et al. 2004), for both the cases of footpoint heating and apex heating. The comparison yields an agreement within  $n_p^{\rm ana}/n_p^{\rm sim}=1.04\pm0.21$ . Thus, our analytical approximations are expected to predict the peak densities  $n_p$  within  $\approx 20\%$  compared with numerical hydrodynamic simulations.

## 2.6. Temperature Profile During the Cooling Phase

After the density peak time  $t_p$ , both the temperature and density are decreasing, as expected when the cooling rate dominates over the declining heating rate. Therefore, we can largely neglect the heating rate for times  $t\gtrsim t_p$  and deal only with losses by thermal conduction (which is proportional to  $T^{7/2}/L^2$ , Equation (9)) and radiation (which is proportional to  $n_e^2$ , Equation (7)). For typical parameters of flare loops, initially the temperature ( $T\gtrsim 10$  MK) is sufficiently high so that

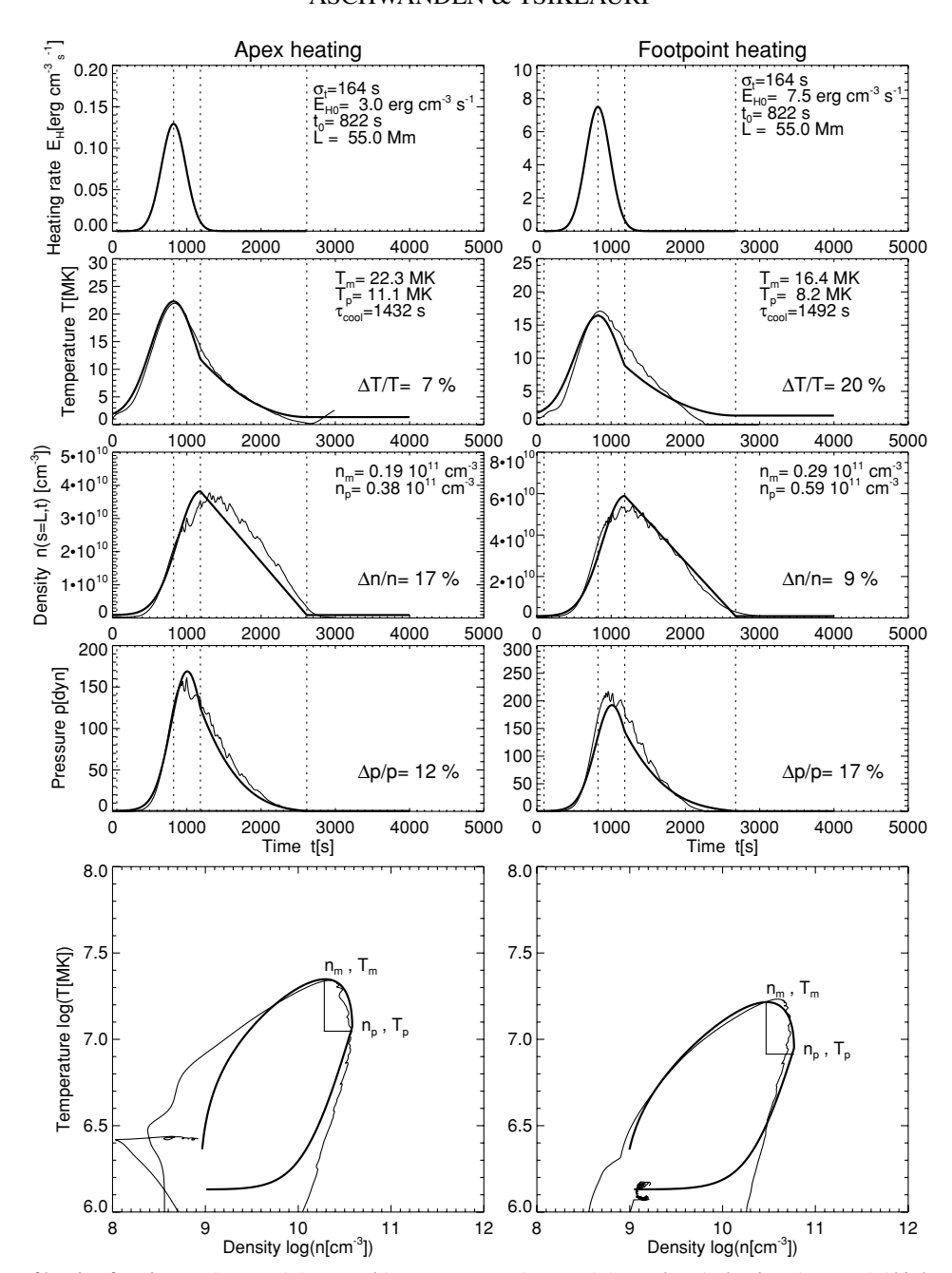


Figure 7. Time evolution of heating function  $E_H(s = L, t)$  (top panels), temperature T(s = L, t) (second row), density n(s = L, t) (third row), pressure p(s = L, t) (fourth row), and logarithmic temperature—density diagram T(n) (bottom panels) of two hydrodynamic simulations from the set of Tsiklauri et al. (2004), for apex heating (left) and footpoint heating (right). The curves of the hydrodynamic simulations are shown with thin linestyle, while our analytical approximations are indicated with thick linestyle. The start time  $t_s$ , temperature maximum time  $t_m$ , density peak time  $t_p$ , and end time  $t_e$  are indicated with dotted vertical lines.

losses by thermal conduction outweigh radiative losses, which generically applies when loops are detected in soft X-rays, while radiative losses dominate later on in the cooling phase, when the temperature drops to  $T \approx 1{\text -}2$  MK, when loops are detected in EUV. Concentrating on the initial hot temperature at the beginning of the cooling phase, neglecting radiative losses in the energy equation, the change in internal energy de(t)/dt) is mainly balanced by the thermal conduction loss rate,

$$mn\frac{de(t)}{dt} = \frac{d}{dt}[3n_e(t)k_BT(t)] = -\frac{d}{ds}\left(\kappa T^{5/2}\frac{dT(t)}{ds}\right)$$

$$\approx -\frac{2}{7}\kappa \frac{T(t)^{7/2}}{L^2},$$
(47)

with  $\kappa$  the *Spitzer* thermal conductivity and L the loop half-length. This differential equation (Equation (46)) can be directly integrated, if we apply the mean-value theorem to the time dependence of the density  $\langle n \rangle \approx n_p$ , yielding

$$T_{\text{cond}}(t) = T_p \left[ 1 + \frac{(t - t_p)}{\tau_{\text{cond}}} \right]^{-2/5}$$
 (48)

with a "conduction timescale"  $\tau_{cond}$  defined by

$$\tau_{\text{cond}}(n = n_p, T = T_p) = \frac{21}{5} \frac{n_p k_B L^2}{\kappa T_p^{5/2}}.$$
(49)

This solution was used in Culhane et al. (1994) to fit the cooling of a flare plasma from  $T_1 = 22$  MK down to 12 MK. Antiochos

& Sturrock (1978) derived a more general cooling function by including the flow and obtained a similar solution (with an exponent of -2/7 rather than -2/5 in Equation (47)).

Later on in the cooling phase, radiative cooling is always dominant, so the internal energy loss de(t)/dt can be equated to the radiative cooling rate,

$$\frac{d}{dt}[3n(t)k_BT(t)] = -n(t)^2\Lambda(T[t]) \approx -n(t)^2\Lambda_0T(t)^{-2/3},$$
(50)

according to the piecewise power-law approximation of the radiative loss function  $\Lambda(T)$  by Rosner et al. (1978). Applying again the mean-value theorem for the time dependence of the density n(t), we can integrate Equation (49) analytically and find the solution

$$T_{\rm rad}(t) = T_p \left[ 1 - \frac{(t - t_p)}{\tau_{\rm rad}} \right]^{3/5},$$
 (51)

with a "radiative cooling time"  $\tau_{rad}$  defined by

$$\tau_{\text{rad}}(n = n_p, T = t_p) = \frac{9k_B T_p^{5/3}}{5n_p \Lambda_0},$$
(52)

where  $\Lambda_0 = 10^{-17.73}$  erg cm<sup>3</sup> s<sup>-1</sup>, since this definition of the radiative cooling time is based on the relation  $\Lambda(T) = \Lambda_0 T^{-2/3}$  as defined for the SXR regime (Equation (8)).

The two phases of dominant conductive cooling and radiative cooling have been combined in subsequent time intervals (e.g., Cargill 1994; Aschwanden & Alexander 2001). A simple combination that is weighted by the shorter timescale is the sum of the reciprocal values,

$$\frac{1}{\tau_{\text{cool}}} = \frac{1}{\tau_{\text{rad}}} + \frac{1}{\tau_{\text{cond}}},\tag{53}$$

which has been used in a number of studies. This definition of the cooling time converges to the value of the conductive cooling timescale (Equation (48)) if  $\tau_{\rm cond} \ll \tau_{\rm rad}$ , or to the value of the radiative cooling timescale (Equation (51)) if  $\tau_{\rm rad} \ll \tau_{\rm cond}$ . For an analytical function that describes the time evolution of the temperature T(t) in the cooling phase, we try several low-order polynomials and find empirically that a quadratic dependence closely matches the temperature profiles obtained in the numerical hydrodynamical simulations of Tsiklauri et al. (2004),

$$T(t) = T_p \left[ 1 - \frac{(t - t_p)}{n_{\text{cool}} \tau_{\text{cool}}} \right]^2 \qquad \text{for } t_p \leqslant t \leqslant t_e \,, \tag{54}$$

which monotonically drops until

$$t_e = t_p + n_{\text{cool}} \tau_{\text{cool}}. \tag{55}$$

The best-matching number of cooling times was found to be  $n_{\rm cool} \approx 3$  for footpoint heating, and  $n_{\rm cool} \approx 4$  for loop apex heating, respectively. The factor  $n_{\rm cool}$  essentially corrects for the time variation of the conductive (Equation (48)) and radiative (Equation (51)) cooling timescales, which both are changing with time  $(t \geqslant t_p)$ , compared with the values calculated at the beginning of the cooling phase  $(t = t_p)$ . We neglect here complicated nonlinear effects in the later cooling phase when the radiative (thermal) instability sets in and catastrophic cooling occurs, which starts below temperatures  $T \lesssim 0.5$  MK where the radiative loss function  $\Lambda(T)$  peaks.

## 2.7. Density Profile during the Cooling Phase

For the evolution of the density n(t) during the cooling phase, we can use the empirical *Jakimiec* (power law) relation

$$\frac{T(t)}{T_p} \approx \left(\frac{n(t)}{n_p}\right)^2,\tag{56}$$

which was found to scale approximately with a power-law slope of  $\approx 2$ , as found in many earlier hydrodynamic simulations (e.g., Jakimiec et al. 1992; Serio et al. 1991; Sylwester et al. 1993; Sylwester 1996). Inserting the temperature evolution in T(t) (Equation (53)) into the Jakimiec's relation (Equation (55)), we obtain a linearly decreasing function:

$$n(t > t_p) \approx n_p \left[ \frac{T(t)}{T_p} \right]^{1/2} = n_p \left[ 1 - \frac{(t - t_p)}{n_{\text{cool}} \tau_{\text{cool}}} \right].$$
 (57)

### 2.8. Summary of Analytical Code

We summarize now the analytical expressions in the order they need to be calculated to provide approximate functions, in explicit form, of the temperature evolution T(s, t) and density n(s, t) for an impulsively heated coronal loop. The free input parameters are the maximum heating rate  $H_{\rm max}$ , the heating timescale  $\tau_{\rm heat}$ , the spatial heating scale height  $s_H$  (which is positive for footpoint heating, negative for apex heating, and infinite for uniform heating), and the loop half-length L. The variables are the space coordinate s, with a range of 0 < s < L for a symmetric loop, and the time coordinate t, within a validity range bound by the start time  $t_s$  and end time  $t_e$ , i.e.,  $t_s < t < t_e$ .

For the analytical calculations, we use the following physical constants: the Boltzmann constant  $k_B = 1.38 \times 10^{-16}$ erg K<sup>-1</sup>, the proton mass  $m_p = 1.67 \times 10^{-24}$  g, the mean molecular weight in the corona  $\mu = 1.27$ , the thermal *Spitzer* conductivity coefficient  $\kappa = 9.2 \times 10^{-7}$  erg s<sup>-1</sup> cm<sup>-1</sup> K<sup>-7/2</sup>, and the radiative loss rate coefficient  $\Lambda_0 = 10^{-17.73} \text{ cm}^3 \text{ s}^{-1}$ (see definition in Equation (8)). Then we first calculate some constants as a function of the free input parameters  $(H_0, \tau_{\text{heat}}, s_H, L)$ , such as the base maximum heating rate  $H_0$ (as defined in Equation (5):  $H_0 = H_{\text{max}}$  for footpoint and uniform heating, and  $H_0 = H_{\text{max}} \exp(-L/s_H)$  for apex heating), the temperature maximum time  $t_m$  (Equation (26)), the density peak time  $t_p$  (Equation (32)), the heating non-uniformity factor  $q_H$  (Equation (21)), the maximum apex temperature  $T_m = T(s = L, t = t_m)$  (Equation (25)), the apex temperature  $T_p = T(s = L, t = t_p)$  at the density peak time (Equation (31)), the *sound speed* at the loop apex and maximum heating time  $t_m$ , i.e.,  $c_s = 1.66 \times 10^4 \left(T_m/10^6 K/\mu\right)^{1/2}$  [cm s<sup>-1</sup>], the RTV loop pressure  $p_1^{\text{RTV}}$  (Equation (35)), Serio's loop base pressure  $p_1^{\text{Serio}}$  (Equation (36)), the pressure scale height  $\lambda_T$ (Equation (37)), Serio's loop apex pressure  $p_2^{\text{Serio}}$  (Equation (38)), Serio's apex density  $n_2^{\text{Serio}}$  (Equation (39)), the chromospheric filling time  $\tau_{\text{fill}}$  (Equation (40)), the dynamic correction factor  $q_n^{\text{dyn}}$  (Equation (42)), the loop apex peak density  $n_p$ (Equation (45)), the evaporation timescale  $\tau_{\text{evap}}$  (Equation (34)), the conductive cooling time  $\tau_{cond}$  (Equation (49)), the radiative cooling time  $\tau_{rad}$  (Equation (51)), and the combined cooling time  $\tau_{\rm cool}$  (Equation (53)).

Now we have all parameter constants and can express the evolution of the temperature profile T(s = L, t) at the loop apex (Equations (24) and (54)),

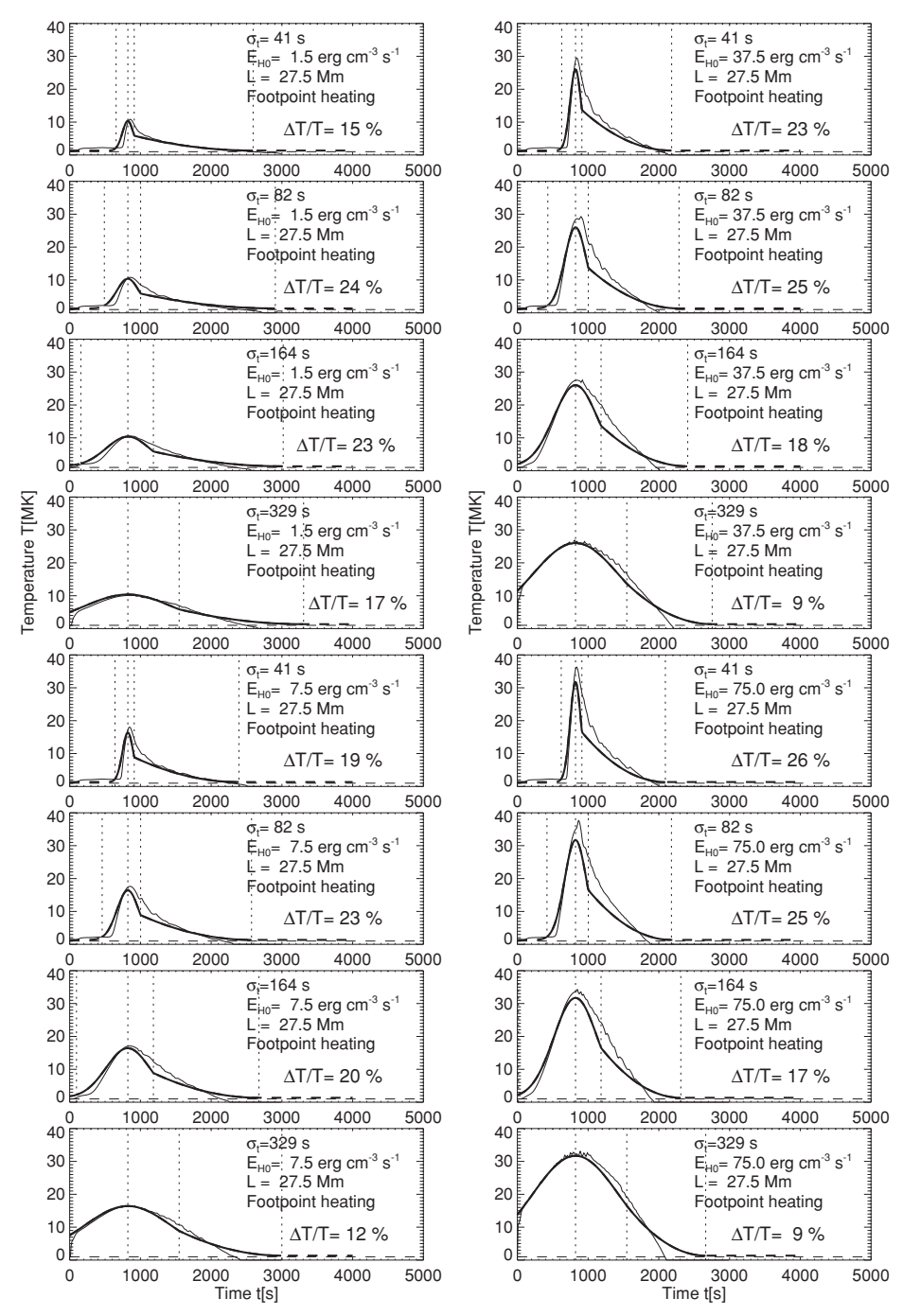


Figure 8. Simulated hydrodynamic temperature profiles T(t, s = L) at the loop apex (thin curves) and analytical approximations (thick curves) for a subset of 56 cases simulated by Tsiklauri et al. (2004). The selected cases include variations of the heating timescale  $t_{\text{heat}}$  and heating rate  $E_H$ , for footpoint heating. The average deviations  $\Delta T/T_{\text{max}}$  between the numerical values and analytical approximations are given in percentages in each frame.

$$T(s = L, t) = \begin{cases} T_m \left[ \exp\left(-(t - t_m)^2 / 7\tau_{\text{heat}}^2\right) \right] & \text{for } t_s \leqslant t \leqslant t_p \\ T_p \left[1 - (t - t_p) / n_{\text{cool}} \tau_{\text{cool}} \right]^2 & \text{for } t_p \leqslant t \leqslant t_e \end{cases}$$
(58)

and the evolution of the density profile n(s = L, t) at the loop apex (Equations (33) and (57)),

$$n(s = L, t)$$

$$= \begin{cases} n_p \exp\left(-(t - t_p)^2 / 2\tau_{\text{evap}}^2\right) & \text{for } t_s \leqslant t \leqslant t_p \\ n_p \left[1 - (t - t_p) / n_{\text{cool}} \tau_{\text{cool}}\right] & \text{for } t_p \leqslant t \leqslant t_e. \end{cases}$$
(59)

The spatial profiles can be approximated with equilibrium solutions (which may be less accurate for short heating rates). The spatial loop profile is then according to the solution given in Equation (22) and the loop apex evolution T(s = L, t) given in Equation (58):

$$T(s,t) = T(s = L, t) \left[ \left( \frac{s}{L} \right) + 2q_H \left( \frac{s_H}{L} \right)^2 \left( 1 - \exp\left( -\frac{s}{s_H} \right) \right) - \left( \frac{s}{L} \right) \left[ 1 - \exp\left( -\frac{L}{s_H} \right) \right] \right]^{2/7}.$$
 (60)

The pressure or density scale height  $\lambda_T$  (Equation (37)) of hydrostatic loops is a function of the temperature, for which we

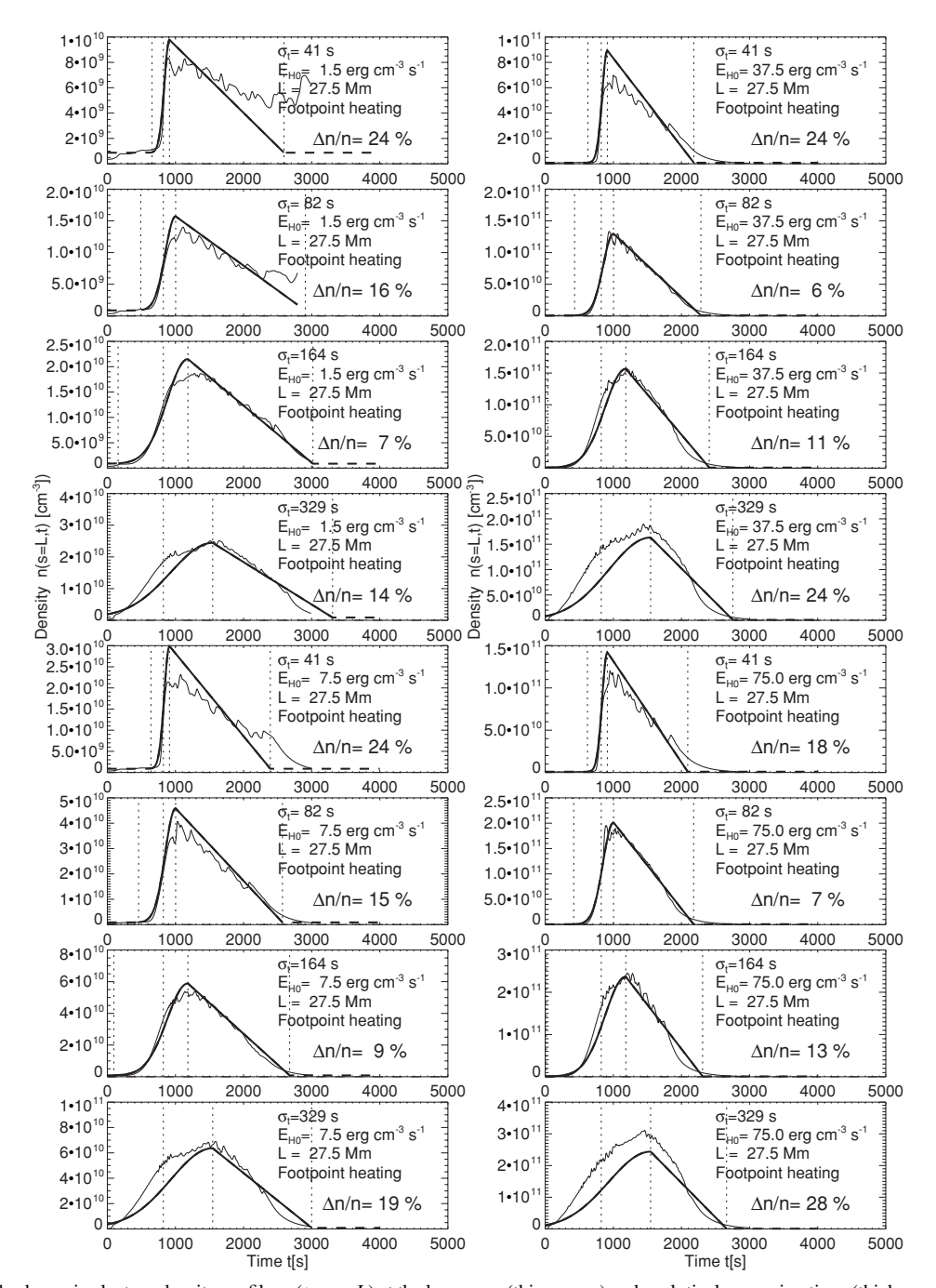


**Figure 9.** Simulated hydrodynamic electron density profiles n(t, s = L) at the loop apex (thin curves) and analytical approximations (thick curves) for the same subset of cases as shown in Figure 8, with similar presentation.

can use approximately the expression for the apex temperature T(s = L, t), yielding (with Equation (38))

$$n(s,t) = n(s = L,t) \left(\frac{T(s = L,t)}{T(s,t)}\right) \times \exp\left(-\frac{h(s) - H}{\lambda_p(T[s = L,t])}\right), \tag{61}$$

where H = h(s = L) is the height of the loop apex. This set of analytical Equations (58)–(61) provides then an complete approximation to the spatiotemporal evolution of loop temperatures T(s, t) and loop densities n(s, t). The validity range of this analytical code is limited to loop apex temperatures in the coronal range of  $T_m \gtrsim 1.0$  MK.

# 3. COMPARISON WITH NUMERICAL HYDRODYNAMIC SIMULATIONS

In this section, we evaluate the accuracy of the analytical approximations computed in the preceding section by comparing the solutions for the temperature T(s, t) and density evolutions n(s, t) with computations from hydrodynamic codes, which are accurate solutions of the time-dependent hydrodynamic equations.

The evolution of heating and cooling in coronal loops was simulated with a 1D radiative hydrodynamic code that incorporates the effects of gravitational stratification, heat conduction, radiative losses, external heat input, inclusion of helium, and Braginskii viscosity in a parametric study with two different (apex and footpoint) heating functions (Tsiklauri et al.

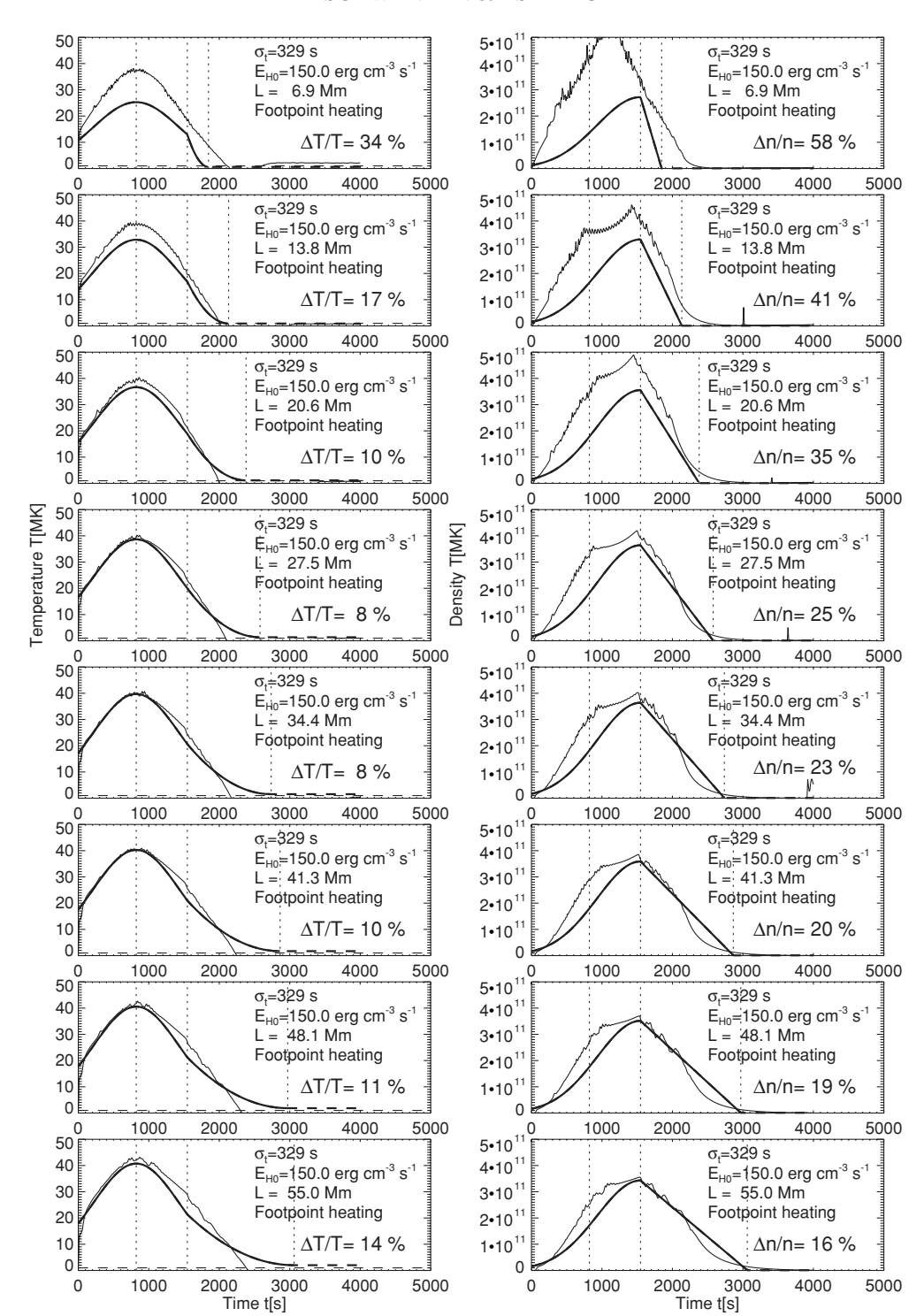


Figure 10. Temperature (left) and density profiles (right) for a subset of cases simulated in Tsiklauri et al. (2004) with varying loop lengths, from L = 13.8 Mm (top) to L = 110 Mm (bottom). Major discrepancies are only found for the shortest loops (top).

2004). The numerical code that we use is a 1D version of the Lagrangian Re-map code (Arber et al. 2001) with radiative loss limiters. One set of 40 simulations was performed with four different heating durations (with Gaussian half-widths of  $\tau_{\text{heat}} = 41, 82, 164, 329 \text{ s}$ ) and five different heating rates ( $H_0 = 0.6, 3, 15, 30, 60 \text{ erg cm}^{-3} \text{ s}^{-1}$ ), for a loop half-length of L = 55 Mm, for both loop apex heating and footpoint heating (localized within a Gaussian width of  $\sigma_s = 7 \text{ Mm}$  from either the apex or footpoint). A second set of 16 sim-

182

ulations was performed for eight different (full) loop lengths (2L = 13.8, 27.5, 41.3, 55.0, 68.8, 82.5, 96.2, 110.0 Mm), for a fixed heating duration of  $\tau_{\text{heat}} = 329 \text{ s}$  and a heating rate of  $H_{\text{max}} = 60 \text{ erg cm}^{-3} \text{ s}^{-1}$  for loop apex heating, and  $H_{\text{max}} = 150 \text{ erg cm}^{-3} \text{ s}^{-1}$  for footpoint heating.

First, we compared the maximum temperatures  $T_m^{\text{ana}} = T(s = L, t = t_m)$  at the loop apex s = L achieved during the entire evolution of a heated loop (at the maximum time  $t = t_m$ ) that we derive in our analytical approximation (Equations (25) and

 Table 1

 Parameters of 56 Hydrodynamic Simulations (Tsiklauri et al. 2004) for Apex and Footpoint Heating, Compared with the Analytical Approximations of Loop Apex Temperature and Densities

Heating Rate $H_{\text{max}}$ (erg cm <sup>-3</sup> s <sup>-1</sup> )	Heating Timescale $\sigma_t$ (s)	Loop Length L (Mm)	Heating Scale Height  SH (Mm)	Simulated Temperature $T_m^{\text{sim}}$ (MK)	Analytical Temperature $T_m^{\text{ana}}$ (MK)	Simulated Density $n_p^{\text{sim}}/10^{10}$ (cm <sup>-3</sup> )	Analytical Density $n_p^{\text{ana}}/10^{10}$ (cm <sup>-3</sup> )	Temperature Ratio $T_m^{\rm ana}/T_m^{\rm sim}$	Density Ratio $n_p^{\text{ana}}/n_p^{\text{sin}}$
0.6	41	27.5	-8.75	13.7	14.1	0.7	0.7	0.98	1.01
0.6	82	27.5	-8.75 -8.75	13.7	14.1	1.1	1.1	0.98	1.02
0.6	164	27.5	-8.75 -8.75	13.8	14.1	1.5	1.1	0.98	1.02
0.6	329	27.5	-8.75 -8.75	13.7	14.1	1.7	1.6	0.97	1.11
3.0	41	27.5	-8.75	22.1	22.3	1.9	2.1	0.99	0.93
3.0	82	27.5	-8.75	22.1	22.3	2.9	3.1	0.99	0.94
3.0	164	27.5	-8.75	21.9	22.3	3.8	3.8	0.98	0.99
3.0	329	27.5	-8.75	21.8	22.3	4.3	4.0	0.98	1.06
15.0	41	27.5	-8.75	35.4	35.3	5.3	6.2	1.00	0.86
15.0	82	27.5	-8.75	35.2	35.3	9.4	8.6	1.00	1.09
15.0	164	27.5	-8.75	34.9	35.3	10.7	10.0	0.99	1.07
15.0	329	27.5	-8.75	35.0	35.3	10.9	10.2	0.99	1.06
30.0	41	27.5	-8.75	43.3	43.0	8.7	9.8	1.01	0.89
30.0	82	27.5	-8.75	43.0	43.0	14.3	13.3	1.00	1.08
30.0	164	27.5	-8.75	42.6	43.0	15.7	15.0	0.99	1.04
30.0	329	27.5	-8.75	42.6	43.0	16.4	15.3	0.99	1.07
60.0	41	27.5	-8.75	52.8	52.4	15.1	15.4	1.01	0.98
60.0	82	27.5	-8.75	53.4	52.5	21.0	20.4	1.02	1.03
60.0	164	27.5	-8.75	52.3	52.5	23.7	22.5	1.00	1.05
60.0	329	27.5	-8.75	52.3	52.5	24.8	22.8	1.00	1.09
1.5	41	27.5	8.75	10.8	10.4	0.8	1.0	1.05	0.85
1.5	82	27.5	8.75	10.8	10.4	1.4	1.6	1.04	0.89
1.5	164	27.5	8.75	10.5	10.4	1.9	2.1	1.02	0.87
1.5	329	27.5	8.75	10.1	10.4	2.5	2.4	0.98	1.03
7.5	41	27.5	8.75	18.0	16.4	2.3	3.0	1.10	0.77
7.5	82	27.5	8.75	17.6	16.4	4.1	4.6	1.07	0.89
7.5	164	27.5	8.75	17.1	16.4	5.4	5.9	1.04	0.92
7.5	329	27.5	8.75	16.5	16.4	6.9	6.4	1.01	1.09
37.5	41	27.5	8.75	29.5	26.0	7.0	8.9	1.13	0.78
37.5	82	27.5	8.75	29.3	26.0	13.3	13.0	1.13	1.03
37.5	164	27.5	8.75	27.6	26.0	15.7	15.7	1.06	1.00
37.5	329	27.5	8.75	26.9	26.0	19.0	16.3	1.03	1.16
75.0	41	27.5	8.75	36.3	31.7	12.1	14.2	1.15	0.85
75.0	82	27.5	8.75	37.7	31.7	19.5	20.2	1.19	0.97
75.0	164	27.5	8.75	34.3	31.7	24.5	23.7	1.08	1.04
75.0	329	27.5	8.75	33.1	31.7	31.1	24.4	1.05	1.28
150.0	41	27.5	8.75	44.5	38.6	21.3	22.5	1.15	0.94
150.0	82	27.5	8.75	45.3	38.6	29.7	31.1	1.17	0.95
150.0	164	27.5	8.75	41.9	38.6	35.0	35.7	1.08	0.98
150.0	329	27.5	8.75	40.2	38.6	41.9	36.4	1.04	1.15
60.0	329	6.9	-8.75	35.2	28.0	37.7	26.1	1.26	1.45
60.0	329	13.8	-8.75	42.1	39.1	33.0	25.4	1.08	1.30
60.0	329	20.6	-8.75	47.7	46.7	28.9	24.1	1.02	1.20
60.0	329	27.5	-8.75	52.3	52.5	24.8	22.8	1.00	1.09
60.0	329	34.4	-8.75	55.5	57.1	23.0	21.6	0.97	1.07
60.0	329	41.3	-8.75	58.8	61.1	21.7	20.5	0.96	1.06
60.0	329	48.1	-8.75	61.2	64.5	18.8	19.5	0.95	0.97
60.0	329	55.0	-8.75	63.6	67.5	18.3	18.6	0.94	0.98
150.0	329	6.9	8.75	38.2	25.3	55.4	27.2	1.51	2.04
150.0	329	13.8	8.75	39.3	32.9	46.1	33.0	1.20	1.40
150.0	329	20.6	8.75	40.4	36.6	48.9	35.5	1.10	1.38
150.0	329	27.5	8.75	40.2	38.6	41.9	36.4	1.04	1.15
150.0	329	34.4	8.75	40.6	39.7	40.2	36.4	1.02	1.11
150.0	329	41.3	8.75	40.9	40.3	38.5	35.9	1.01	1.07
150.0	329	48.1	8.75	42.6	40.6	37.0	35.1	1.05	1.05
150.0	329	55.0	8.75	43.1	40.7	35.6	34.3	1.06	1.04

(58)) with the numerically obtained temperature maxima  $T_m^{\text{sim}}$  (Figure 3). Note that the theoretical expression for the maximum temperature  $T_m$  (Equation (25)) depends only on the maximum

heating rate  $H_0$ , loop length L, and heating scale height  $s_H$ . Note that the footpoint heating rate  $H_0$  used in Equation (25) is related to the apex heating rate  $H_{\text{max}}$  of the numerical simulation

by Equation (5). The spatial heating function is described with a Gaussian with width  $\sigma_s$  in the numerical simulations of Tsiklauri et al. (2004), while we parameterize it with an exponential scale height  $s_H$ . Constraining the two slightly different spatial heating functions by the same maximum value and integral value yields the conversion  $s_H \approx 1.25\sigma_s$ . The comparison is shown in Figure 3 for 56 numerical simulations, where we find that the 56 cases within  $T_m^{\rm ana}/T_m^{\rm sim}=0.96\pm0.07$ . The remaining small differences may be attributed to the slightly different definitions of the spatial heating function or to the effects of dynamic flows and radiative losses neglected in the analytical approximation. The simulated and analytical values for the maximum temperatures and peak densities are also listed in Table 1.

Second, we compared the peak densities  $n_p^{\rm ana}=n(s=L,t=t_p)$  at the loop apex s=L and peak time  $t=t_p$  that we derived in our analytical approximation (Equations (46) and (59)) with the numerically obtained maxima  $n_p^{\rm sim}$  (Figure 6). The comparison with the 56 numerical simulations shown in Figure 6 shows a good agreement of these peak densities, which agree within  $n_p^{\rm ana}/n_p^{\rm sim}=1.04\pm0.21$ . This agreement in density within  $\lesssim 20\%$  is relatively good, given that density fluctuations associated with dynamic flows in impulsively heated loops are of the same magnitude.

In Figures 7–10, we show comparisons of time profiles computed with our analytical code versus numerical hydrodynamic simulations of Tsiklauri et al. (2004). The time profiles of the heating rate  $E_H(t)$ , temperature evolution T(t,s=L), density evolution n(t,s=L), pressure evolution p(t,s=L), and temperature—density phase diagram T(n) are shown for two cases with apex and footpoint heating in Figure 7. To each time profile we quantify also the mean deviations between the analytical and numerical solutions, i.e.,  $\Delta T/T_{\rm max}$ ,  $\Delta n/n_{\rm max}$ , and  $\Delta p/p_{\rm max}$ , which are all of the order  $\approx$ 20%. These mean deviations are also listed for all 56 cases in Table 1.

In Figure 8, we show the temperature profiles of 18 cases with various heating timescales and heating rates (with footpoint heating). The corresponding 18 density profiles are shown in Figure 9. In Figure 10, we show the temperature and density profiles of a subset of Tsiklauri et al.'s (2004) simulations with varying loop lengths (2L = 14-110 Mm). We see that the analytical time profiles agree with the numerically simulated time profiles in the average with an accuracy of about  $\lesssim 20\%$  in temperature and density, similar to the agreement of the maximum values (Figures 3 and 6). The analytical approximations can therefore be considered as sufficiently accurate for most practical applications in the parameter regime explored by Tsiklauri et al. (2004), which ranges from hot active region loops to the hottest flare loops. Moreover, our approximations apply to uniform as well as to non-uniform (footpoint and apex) heating. The numeric code of these analytical approximations can be requested from the author in the form of IDL procedures.

## 4. CONCLUSIONS

We developed a simple analytical approximation of the hydrodynamic evolution of the temperature T(s,t) and electron density n(s,t) for an impulsively heated and subsequently cooling coronal loop. The analytical approximation is expressed in explicit form as a function of the input parameters of the temporal and spatial heating function, such as the maximum heating rate  $H_{\text{max}}$ , the heating timescale  $\tau_{\text{heat}}$ , the spatial heating

scale height  $s_H$ , and the loop length L. The analytical solution is generalized for both uniform and non-uniform (exponentially decreasing) spatial heating functions. The analytical expressions are derived from the hydrodynamic energy and momentum equation, complemented with the loop scaling laws of RTV and Serio, the Neupert effect, and the empirical Jakimiec relationship. The assumptions of our analytical model include (1) the heating rate is a symmetric (e.g., Gaussian) function in time, (2) losses by thermal conduction are dominant during the heating phase, (3) chromospheric evaporation is characterized by the Neupert effect and describes the density increase during the heating, (4) thermal conduction dominates the initial cooling phase, and (5) the density decrease during the cooling phase is characterized by the Jakimiec relation,  $T \propto n^2$ . The analytical approximations are tested with the numerical hydrodynamic simulations of a parametric study (Tsiklauri et al. 2004) that covers a large parameter space of heating functions, mostly relevant for flare loops. The analytical approximations match the numerical simulations with an accuracy of  $\approx$ 20% in temperature and

Some caveats have to be made for the validity of the approximations derived here. The validation is only based on 56 numeric hydrodynamic simulations by Tsiklauri et al. (2004), which were mostly designed for flaring conditions (i.e., high heating rates, maximum temperatures in the range of  $T \approx 10-50$  MK). That parametric study includes apex and footpoint heating only, but no uniform heating. The hydrodynamic code of Arber et al. (2001) used in Tsiklauri et al. (2004) has not been compared with other codes yet, but a major benchmarking program is in progress (A. Winebarger 2009, private communication). Regarding the analytical treatment, we neglected flows, kinetic energy, and the gravitational potential in the energy equation, but a time dependence of the loop filling is included in the density evolution (Equation (42)). Some of the neglected effects are corrected by empirical constants, that are optimized for the Tsiklauri data set, but may slightly change when compared with other numerical simulations. We plan a major parametric study with the EBTEL code (Klimchuk et al. 2008), which is a very fast code, but is restricted to uniform heating and parameters averaged over the loop length.

The analytical expressions derived here can be used to efficiently model the hydrodynamic evolution of coronal loops and flare loops. The analytical density n(s, t) and temperature evolutions T(s, t) can easily be convolved with an instrumental temperature response function R(T) in order to simulate light curves of multi-wavelength observations in EUV and soft X-rays. Forward fitting of our simple analytical expressions to observed light curves in various temperature filters can then be used straightforwardly to infer the underlying spatial and temporal heating function of coronal loops. Superimposing the evolutions of multiple loops can mimic flare light curves. Summing the evolutions of light curves from an ensemble of loops with suitable distribution functions of geometric loop parameters can easily reproduce DEM distributions of an active region, the full Sun, or the solar or stellar irradiance. In all these applications, analytical expressions in explicit form of the heating function are a key tool to model the observed light curves, which would not be practicable with numerical hydrodynamic simulations, the only tool we had at hand so far. We think, therefore, that these analytical functions are valuable tools for future modeling and interpretation of soft X-ray and EUV multi-wavelength data from the TRACE, SOHO, STEREO, Hinode, and SDO missions.

The analytical code is available as IDL procedures (HYDRO\_APPROX1.PRO and HYDRO\_APPROX2.PRO) in the *Solar Software (SSW)* library. Interested users can also request a copy from the first author.

The authors are most indebted to Tony Arber for providing the code of the numerical hydrodynamic simulations. We acknowledge also valuable and inspiring discussions with Jim Klimchuk, Harry Warren, Amy Winebarger, Barbara Sylwester, and other participants of the three *Coronal Loop Modeling* workshops in Paris, France (2002 November 13–15), in Palermo, Sicily (2004 August 1–3), and in Santorini, Greece (2007 June 18–21). Part of this work was supported by NASA contract NAS5-38099 (*TRACE* mission).

### **REFERENCES**

```
Antiochos, S. K., & Sturrock, P. A. 1978, ApJ, 220, 1137
Arber, T. D., Longbottom, A. W., Gerrard, C. L., & Milne, A. M. 2001, J.
    Comput. Phys., 171, 151
Aschwanden, M. J. 2004, Physics of the Solar Corona - An Introduction (New
   York: Springer)
Aschwanden, M. J., & Alexander, D. A. 2001, Sol. Phys., 204, 91
Betta, R. M., Orlando, S., Giovanni, P., & Serio, S. 1999, Space Sci. Rev., 87,
Bloomberg, H. W., Davis, J., & Boris, J. P. 1977, JQSRT, 18, 237
Brown, J. C. 1973, Sol. Phys., 31, 1973
Cargill, P. J. 1994, ApJ, 422, 381
Cargill, P. J., & Klimchuk, J. A. 2004, ApJ, 605, 911
Cargill, P. J., & Priest, E. R. 1980, Sol. Phys., 65, 251
Cheng, C. C., Tandberg-Hanssen, E., & Orwig, L. E. 1984, ApJ, 278, 853
Craig, I. J. D., Robb, T. D., & Rollo, M. D. 1982, Sol. Phys., 76, 331
Culhane, J. L., et al. 1994, Sol. Phys., 153, 307
Falchi, A., & Mauas, P. J. D. 2002, A&A, 387, 678
Fisher, G. H. 1989, ApJ, 346, 1019
Fisher, G. H., Canfield, R. C., & McClymont, A. N. 1985a, ApJ, 289, 414
Fisher, G. H., Canfield, R. C., & McClymont, A. N. 1985b, ApJ, 289, 425
Fisher, G. H., Canfield, R. C., & McClymont, A. N. 1985c, ApJ, 289, 434
Fisher, G. H., & Hawley, S. L. 1990, ApJ, 357, 243
Gan, W. Q., Zhang, H. Q., & Fang, C. 1991, A&A, 241, 618
Jakimiec, J., Sylwester, B., Sylwester, J., Serio, S., Peres, G., & Reale, F. 1992,
   A&A, 253, 269
Klimchuk, J. A., Antiochos, S. K., & Mariska, J. T. 1987, ApJ, 320, 409
Klimchuk, J. A., & Mariska, J. T. 1988, ApJ, 328, 334
```

```
Kopp, R. A., & Poletto, G. 1993, ApJ, 418, 496
Krall, K. R., & Antiochos, S. K. 1980, ApJ, 242, 374
MacNeice, P. 1986, Sol. Phys., 103, 47
MacNeice, P., McWhirter, R. W. P., Spicer, D. S., & Burgess, A. 1984, Sol.
   Phys. 90, 357
Mariska, J. T., & Boris, J. P. 1983, ApJ, 267, 409
Mariska, J. T., Emslie, A. G., & Li, P. 1989, ApJ, 341, 1067
Mariska, J. T., & Poland, A. I. 1985, Sol. Phys., 96, 317
McClymont, A. N., & Craig, I. J. D. 1985a, ApJ, 289, 834
McClymont, A. N., & Craig, I. J. D. 1985b, ApJ, 289, 820
Mok, Y., Schnack, D. D., & VanHoven, G. 1991, Sol. Phys., 132, 95
Nagai, F. 1980, Sol. Phys., 68, 351
Nagai, F., & Emslie, A. G. 1984, ApJ, 279, 896
Noci, G. 1981, Sol. Phys., 69, 63
Pallavicini, R., & Peres, G. 1983, Sol. Phys., 86, 147
Parker, E. N. 1958, ApJ, 128, 664
Peres, G. 1997, in ESA-SP 404, Fifth SOHO Workshop: The Corona and Solar
   Wind Near Minimum Activity, ed. A. Wilson (Noordwijk: ESA), 55
Peres, G., Serio, S., Vaiana, G. S., & Rosner, R. 1982, ApJ, 252, 791
Priest, E. R., Foley, C. R., Heyvaerts, J., Arber, T. D., Mackay, D., Culhane, J.
   L., & Acton, L. W. 2000, ApJ, 539, 1002
Reale, F., Peres, G., Serio, S., Betta, R., DeLuca, E. E., & Golub, L. 2000a, ApJ,
Reale, F., Peres, G., Serio, S., DeLuca, E. E., & Golub, L. 2000b, ApJ, 535, 412
Robb, T. D., & Cally, P. S. 1992, ApJ, 397, 329
Rosner, R., Tucker, W. H., & Vaiana, G. S. 1978, ApJ, 220, 643
Serio, S., Peres, G., Vaiana, G. S., Golub, L., & Rosner, R. 1981, ApJ, 243,
Serio, S., Reale, F., Jakimiec, J., Sylwester, B., & Sylwester, J. 1991, A&A,
   241, 197
Somov, B. V., Sermulina, B. J., & Spektor, A. R. 1982, Sol. Phys., 81, 281
Somov, B. V., Syrovatskii, S. I., & Spektor, A. R. 1981, Sol. Phys., 73, 145
Spadaro, D., Lanza, A. F., Lanzafame, A. C., Karpen, J. T., Antiochos, S. K.,
   Klimchuk, J. A., & MacNeice, P. J. 2003, ApJ, 582, 486
Sylwester, B. 1996, Space Sci. Rev., 76, 319
Sylwester, B., Sylwester, J., Serio, S., Reale, F., Bentley, R. D., & Fludra, A.
   1993, A&A, 267, 586
Tsiklauri, D., Aschwanden, M. J., Nakariakov, V. M., & Arber, T. D. 2004, A&A,
   419, 1149
Veronig, A. M., Brown, J. C., Dennis, B. R., Schwartz, R. A., Sui, L., & Tolbert,
   K. 2005, ApJ, 621, 482
Vesecky, J. F., Antiochos, S. K., & Underwood, J. H. 1979, ApJ, 233, 987
Warren, H. P., Winebarger, A. R., & Hamilton, P. S. 2002, ApJ, 579, L41
Winebarger, A. R., & Warren, H. P. 2004, ApJ, 610, L129
Winebarger, A. R., & Warren, H. P. 2005, ApJ, 626, 543
Winebarger, A. R., Warren, H. P., & Mariska, J. T. 2003a, ApJ, 587, 439
Winebarger, A. R., Warren, H. P., & Seaton, D. B. 2003b, ApJ, 593, 1164
```

Klimchuk, J. A., Patsourakos, S., & Cargill, P. J. 2008, ApJ, 682, 1351